Electronic states of RFe$_2$O$_4$ (R = Lu, Yb, Tm, Y) mixed-valence compounds determined by soft x-ray absorption spectroscopy and x-ray magnetic circular dichroism

Sara Lafuerza,[1,*] Joaquín García,[2] Gloria Subías,[2] Javier Blasco,[2] Javier Herrero-Martín,[3] and Sakura Pascarelli[1]

[1]*European Synchrotron Radiation Facility (ESRF), CS40220, F-38043 Grenoble Cedex 9, France*
[2]*Instituto de Ciencia de Materiales de Aragón, Departamento de Física de la Materia Condensada,
CSIC-Universidad de Zaragoza, Zaragoza, 50009, Spain*
[3]*ALBA Synchrotron, Ctra. BP1413 km 3.3, 08290 Cerdanyola del Vallès, Barcelona, Spain*

We here report an investigation of the electronic states in the RFe$_2$O$_4$ (R = Lu, Yb, Tm, Y) mixed-valence ferrites by means of soft x-ray absorption spectroscopy (XAS) and x-ray magnetic circular dichroism (XMCD) measurements together with *ab initio* theoretical calculations. The presence of Fe^{+2} and Fe^{+3} pure ionic species is discarded in the XAS spectra at the O K edge in both experimental data and simulations based on the multiple scattering theory. Similarly, no trace of Fe^{+2}/Fe^{+3} contributions is detected in the XMCD spectra at the Fe K edge. On the other hand, the XAS and XMCD spectra at the Fe $L_{2,3}$ edges can be well described in terms of Fe^{+2}/Fe^{+3} contributions, and are also supported by multiplet calculations. This finding can be interpreted as the existence of a mixture of $3d^5$/$3d^6$ configurations at the Fe atoms. Alternative ferrimagnetic spin orderings based on a trimodal Fe valence distribution are also proposed and discussed. Finally, a possible explanation for the strong dependence of the Fe $L_{2,3}$ edges XMCD signal magnitude on both the sample surface preparation and detection method is presented.

I. INTRODUCTION

Mixed-valence transition-metal oxides exhibit remarkable properties such as high temperature superconductivity, colossal magnetoresistance, and multiferroicity, which may give rise to important technological applications [1]. Their interesting features are the result of the complex coupling between spin, charge, lattice, and orbital degrees of freedom. In particular, multiferroic materials that offer the possibility of simultaneously controlling magnetic and electric orderings are nowadays the subject of intense interest as they could lead to new types of multifunctional devices [2]. The mixed-valence ferrites RFe$_2$O$_4$ (R = rare earths from Ho to Lu and Y) have been known for more than three decades [3]. Recently, their structural, magnetic, and dielectric properties, in particular that of LuFe$_2$O$_4$, have attracted renewed interest in the field of multiferroicity [4–8].

The RFe$_2$O$_4$ compounds show different physical properties and structural phase transitions depending on the type of R^{+3} cation. At high temperature all of them adopt a rhombohedral structure (space group $R\bar{3}m$) [9], which can be alternatively described in the hexagonal setting. Along the hexagonal c axis, the structure can be seen as a sequence of Fe-O double layers forming two-dimensional triangular layers separated by a single R-O layer (we note that from here, the hexagonal setting will be used). This structure is stable down to 80 K for YbFe$_2$O$_4$ and TmFe$_2$O$_4$, whereas LuFe$_2$O$_4$ exhibits two structural transitions upon cooling down [10]. It undergoes a first transition at 320 K from hexagonal to monoclinic (space group $C2/m$) and a second transition near 200 K from monoclinic to triclinic (space group $P\bar{1}$). On the other hand, the YFe$_2$O$_4$ compound shows a complex low temperature structure with various crystal distortions coupled

to two successive Verwey-type metal-insulator transitions at about 240 and 190 K [11,12] not observed in the Lu, Yb, and Tm compounds. Concerning the magnetic properties, LuFe$_2$O$_4$ [13,14], YbFe$_2$O$_4$ [15], and TmFe$_2$O$_4$ [16] exhibit ferrimagnetic ordering below $T_N \approx 240-250$ K, whereas the YFe$_2$O$_4$ compound is antiferromagnetic [11].

The most studied compound of the RFe$_2$O$_4$ family is by far LuFe$_2$O$_4$ since it was claimed to be multiferroic with a novel type of ferroelectricity based on Fe^{+3}/Fe^{+2} charge ordering (CO) below $T_{CO} \approx 320$ K [17]. Ferroelectricity in LuFe$_2$O$_4$ was proposed on the basis of the observed colossal dielectric response and polarization measurements obtained by the pyroelectric current detection method [5,7]. Moreover, giant room temperature magnetodielectric response was reported in a LuFe$_2$O$_4$ single crystal [8]. Resonant x-ray scattering (RXS) experiments at the Fe K edge [17] were interpreted as the experimental proof of the Fe^{+3}/Fe^{+2} CO. Immediately the CO was considered to be a new mechanism for the origin of ferroelectricity, and a large number of papers aiming at understanding this phenomenology in LuFe$_2$O$_4$ were published following the CO ionic model [18–38]. Despite the widespread belief in the existence of ferroelectricity in LuFe$_2$O$_4$, recent results have challenged both the polar character and the existence of pure ionic CO. It has been demonstrated that the colossal dielectric permittivity is originated by the electrical contacts [39–41] and that LuFe$_2$O$_4$ does not show spontaneous electrical polarization in the $P(\mathbf{E})$ loops [41]. In addition, x-ray absorption spectroscopy (XAS) experiments at the Fe K edge have shown that the charge segregation between the different iron atoms cannot be larger than 0.5 electrons [42]. New RXS experiments [43,44] have elucidated the existence of two ordered phases below T_{CO}, in agreement with the $C2/m$ and $P\bar{1}$ symmetries with four-modal and trimodal Fe charge distributions, respectively, being the valence segregation considerably smaller than one electron for both phases. Furthermore, high resolution x-ray

_____

*E-mail: sara.lafuerza@esrf.fr

synchrotron powder diffraction results have corroborated the nonpolar crystal structure and the small charge segregation [10,43]. Therefore, Fe^{+2}/Fe^{+3} CO leading to a polar configuration in $LuFe_2O_4$ lacks experimental support. These results suggest that the Fe atoms in the mixed-valence RFe_2O_4 compounds are in a homogeneous mixed-valence state (i.e., their electronic configuration is intermediate between Fe^{+3} and Fe^{+2}) instead of a heterogeneous mixed-valence state between two integer valences. The latter applies to both the symmetric high temperature phase and the so-called CO phases. This phenomenology is shared with other archetypical CO compounds like magnetite [45] or some mixed-valence manganites [46]. Previous to these recent results, various x-ray magnetic circular dichroism (XMCD) experiments at the Fe $L_{2,3}$ edges in $LuFe_2O_4$ [27,30,38] were interpreted using a spin ordering model in terms of the Fe^{+2}/Fe^{+3} ionic species in which all Fe^{+2} as well as 1/3 of the Fe^{+3} moments are aligned parallel to the applied magnetic field and the remaining 2/3 of the Fe^{+3} in an antiparallel way.

In view of these results, a consistent description of the local electronic and magnetic structure of the RFe_2O_4 compounds in the new framework of homogeneous intermediate valence state for the Fe atoms is mandatory. In order to address this issue, we have performed a characterization of $LuFe_2O_4$ by means of soft XAS measurements at the O K edge and Fe $L_{2,3}$ edges in combination with XMCD measurements at both Fe $L_{2,3}$ and K edges. Samples of other RFe_2O_4 (R = Yb, Tm, Y) mixed-valence ferrites and the isostructural $LuFeCoO_4$ compound [9] have been also studied in order to obtain a general description of the series. Regarding the formerly reported XAS/XMCD works in $LuFe_2O_4$, we here present the following results: (i) a complete XAS characterization at the O K edge and Fe $L_{2,3}$ edges since our data include RFe_2O_4 (R = Yb, Tm, Y) and $LuFeCoO_4$ samples, (ii) XMCD spectra at the Fe $L_{2,3}$ edges with the magnetic field applied both parallel and perpendicular to the c axis, and (iii) XMCD spectra at the Fe K edge, not reported before to the best of our knowledge.

II. EXPERIMENTAL AND CALCULATION DETAILS

Polycrystalline powders of RFe_2O_4 (R = Lu, Yb, Tm, Y) were obtained by solid state chemistry reaction from stoichiometric amounts of R_2O_3 and Fe_2O_3 (more details can be found in Ref. [42]). Similarly, $LuFeCoO_4$ powder samples were prepared in air at 1350 ºC using Lu_2O_3, Fe_2O_3, and CoO as precursors. A $LuFe_2O_4$ single crystal was grown by the optical floating zone method (more details can be found in Ref. [41]). All samples were analyzed by x-ray diffraction being single phase. Magnetic measurements were carried out between 5 and 300 K using a commercial Quantum Design superconducting quantum interference device (SQUID) magnetometer. Figure 1 shows the temperature dependence of the zero-field-cooled (ZFC) and field-cooled (FC) magnetization for various RFe_2O_4 samples (R = Lu, Yb, Tm) and applied magnetic field (**H**) of either 4 T or 5 T. The ZFC-FC magnetic irreversibility at low temperatures and the strong anisotropy with an easy magnetic direction parallel to the crystallographic c axis agree with previous reports in the literature [13–16]. We would like to emphasize that magnetization reversal can only be achieved, for a given **H**, at temperatures where the ZFC-FC

curves overlap. We note that the XMCD signal obtained by inverting **H** at temperatures in the regime of ZFC-FC irreversibility will be near zero because then the magnetic field is not able to invert the magnetization. All the samples show a sharp transition at $T_N \approx 250-240$ K for $H = 0.1$ T (not shown here), in agreement with the expected ferrimagnetic ordering and a large low temperature coercivity. Thermal and electrical properties as a function of temperature for the studied RFe_2O_4 (R = Lu, Yb, Tm, Y) samples show the anomalies at the phase transition temperatures expected for stoichiometric compounds [10,41,42].

Measurements of soft XAS at both the O K edge and Fe $L_{2,3}$ edges together with XMCD at the Fe $L_{2,3}$ edges were carried out at the BOREAS beamline [47] of the ALBA synchrotron light source (Barcelona, Spain) on a single crystal of $LuFe_2O_4$ and polycrystalline samples of RFe_2O_4 (R = Lu, Yb, Tm, Y) and $LuFeCoO_4$ (in this case, XAS measurements at the Co $L_{2,3}$ edges were also performed) using the high-field vector magnet end-station. The anisotropy in the XAS was probed in the $LuFe_2O_4$ single crystal by measuring polarized spectra with the x-rays polarization vector (**E**) parallel and perpendicular to the c axis. All samples were polished *in situ* under ultrahigh vacuum conditions ($\approx 10^{-8}$ mbar) unless otherwise stated. In particular, one polycrystalline sample of $LuFe_2O_4$ was cleaved in order to check the dependence of the XAS/XMCD spectral shape on the surface cleaning process. The absorption intensity was measured by simultaneous detection of the total electron yield (TEY) and the fluorescence yield (FY). In the TEY detection, the electron intensity was measured using an electrometer, while for the FY detection a photodiode located at 90° with respect to the x-ray beam direction was used. The surface of the polycrystalline samples was aligned at 45° with respect to the photodiode and in the case of the single crystal samples at 20–30° in order to have a component of the magnetic field in the crystallographic direction of interest. For the XMCD measurements, a magnetic field of magnitude $H = 4$ T was applied collinearly to the x-ray beam propagation direction, and samples were cooled down to 150 K. The FY detected XAS spectra at the Fe $L_{2,3}$ edges are strongly affected by self-absorption (SA), but we have developed a method to correct for it that makes use of the SA-free TEY spectra, as described in the Appendix.

The XAS and XMCD measurements at the Fe K edge were performed at the ID24 beamline [48] of the ESRF (Grenoble, France) on oriented powder samples of RFe_2O_4 (R = Lu, Yb) (the preparation method for the oriented samples is described in Ref. [42]). Data were collected in transmission mode under $H \approx 1$ T in a temperature range between 45 K and 200 K. Circular polarization was attained using a diamond quarter wave plate.

All the x-ray absorption near edge structure (XANES) spectra (O K edge, Fe $L_{2,3}$ edge, and Fe K edge) presented have been normalized by first subtracting the linear pre-edge contribution and fixing the jump to one at values well above the absorption edge. Then, the XMCD signals have been obtained as the difference between the normalized absorption spectra measured with right and left helicity of the incoming circularly polarized light, respectively.

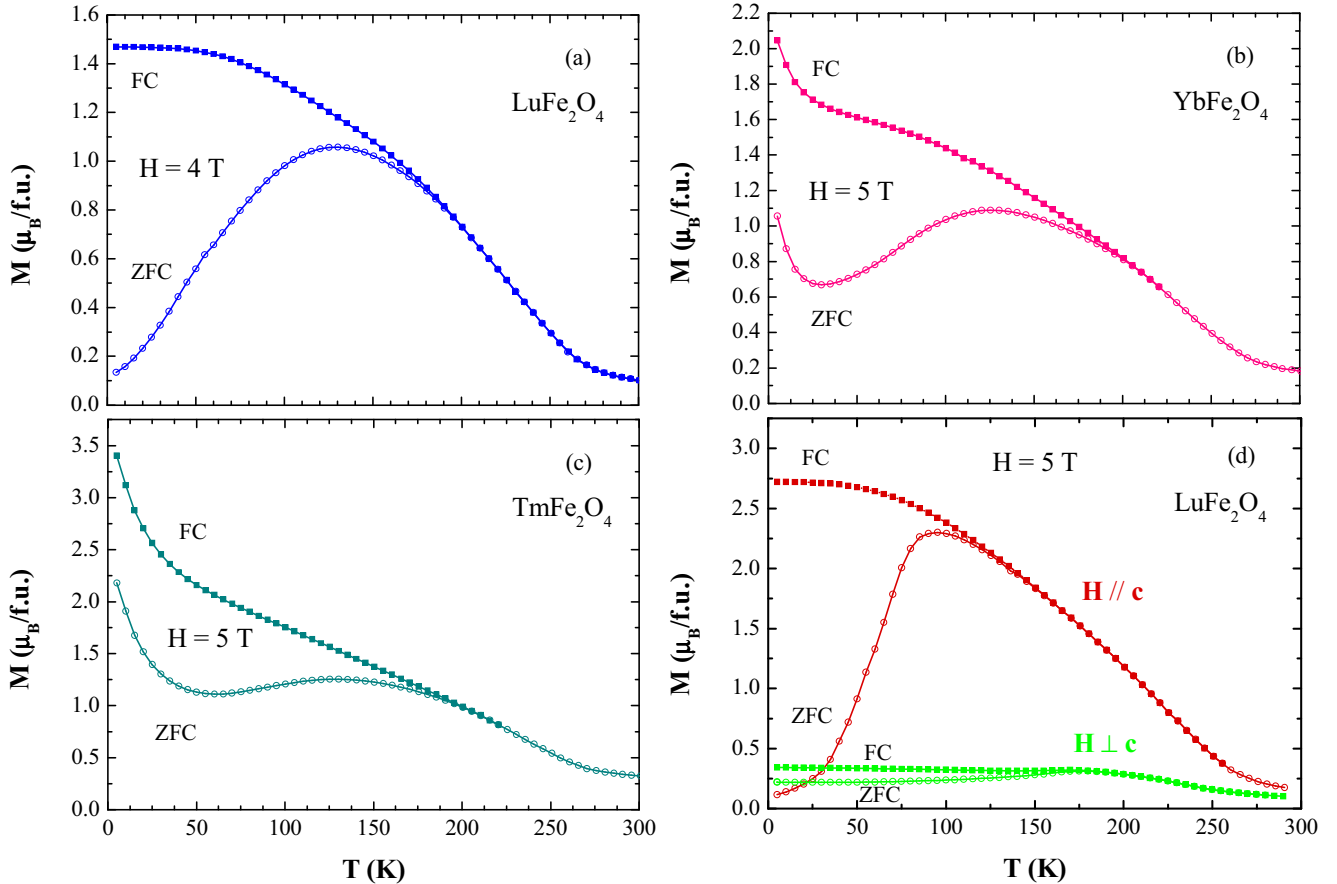Theoretical calculations of the XANES spectra at the O K edge of $LuFe_2O_4$ were performed using the FDMNES

FIG. 1. (Color online) Temperature dependence for magnetization of (a) LuFe$_2$O$_4$, (b) YbFe$_2$O$_4$, and (c) TmFe$_2$O$_4$ polycrystalline samples and (d) LuFe$_2$O$_4$ single crystal. In the latter, data with applied magnetic field **H** both parallel (easy axis) and perpendicular (hard axis) to the hexagonal c axis are shown. In all the panels, ZFC (open symbols) and FC (closed symbols) stand for zero-field-cooled and field-cooled magnetization, respectively.

code [49] in the multiple scattering (MS) real-space approach within the muffin-tin approximation for the potential. The exchange-correlation part of the potential was taken as the real Hedin, Lundqvist, and von Barth potential, and the spectra were convoluted using an appropriate Lorentzian function. The high temperature hexagonal cell of LuFe$_2$O$_4$ [9] with two nonequivalent oxygen atoms O1(6c) and O2(6c) was employed to obtain the atomic positions. On the other hand, simulations of XANES and XMCD spectra at the Fe $L_{2,3}$ edges were performed in the framework of the multiplet theory [50] by using the CTM4XAS code [51]. In this case, XANES simulations were independently carried out for Fe^{+2} and Fe^{+3} ions. We used a Slater integral reduction of 1%, and we set C$_{3i}$ symmetry (as corresponds to a FeO$_5$ trigonal pyramid) and a splitting energy 10 Dq = 1 eV as crystal field parameters. X-ray magnetic circular dichroism simulations were carried out at $T = 0$ K, with a Zeeman splitting of 1 meV.

III. RESULTS

A. XANES at the O K edge

Figure 2(a) compares the XANES spectra of the same polycrystalline LuFe$_2$O$_4$ sample recorded in TEY and FY. The two detection methods yield comparable spectra; therefore,

they guarantee that surface and bulk are equivalent. Hereafter, all the spectra that will be shown correspond to the TEY detection unless otherwise said. The XANES spectra of the mixed-valence RFe$_2$O$_4$ ($R =$ Lu, Yb, Tm, Y) and LuFeCoO$_4$ polycrystalline samples are shown in Fig. 2(b). We observe that the spectral line shapes are very similar along the $R =$ Lu, Yb, and Tm series and also with respect to the LuFeCoO$_4$ reference compound, with Fe^{+3} formal valence. A small difference is observed in the energy position of the second and third peaks between the $R =$ Y compound and all the other samples. This indicates that the O $2p$ states mix with both the Fe $3d$ states and rare earth $5d$ states in a similar fashion in all these systems. In the case of the YFe$_2$O$_4$ compound, the different spectral line shape can instead be explained as due to the O $2p$ states mixing with the Y $4d$ states. Finally, the polarized spectra measured on the LuFe$_2$O$_4$ single crystal for the two configurations **E** // **c** and **E** $\perp$ **c** are displayed in Fig. 2(c). We note that our polarized spectra agree with the published ones by Ko *et al.* [27]. The anisotropy in the XANES at the O K edge between **E** // **c** and **E** $\perp$ **c** is weak, indicating that the strong crystallographic anisotropy is hardly reflected on the O $p-$projected density of states. This weak local anisotropy has been also observed in the XANES at the Fe K edge for the RFe$_2$O$_4$ ($R =$ Lu, Y, Yb) and LuFeCoO$_4$
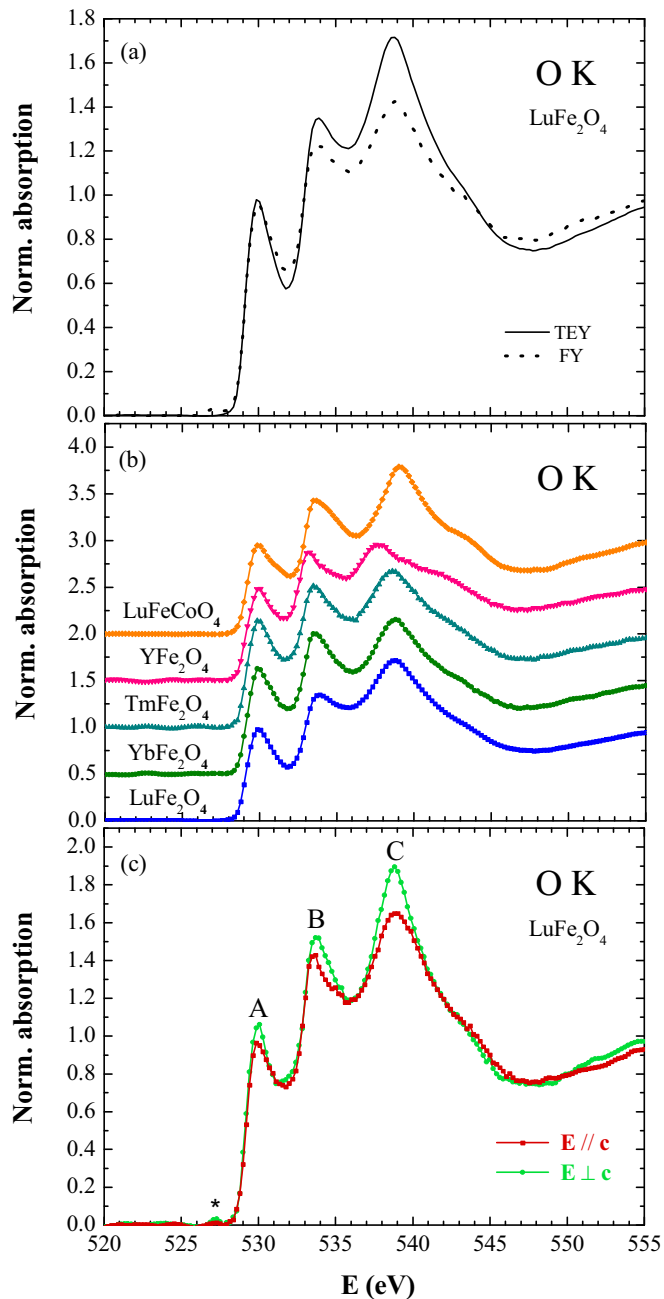
FIG. 2. (Color online) Normalized XANES spectra at the O K edge measured at room temperature. (a) Comparison between the spectra measured by TEY and FY for a $LuFe_2O_4$ polycrystal. (b) Spectra measured by TEY for the RFe_2O_4 (R = Lu, Yb, Tm, and Y) and $LuFeCoO_4$ polycrystalline samples shifted in vertical for the sake of comparison. (c) Polarized XANES spectra measured by TEY for the $LuFe_2O_4$ single crystal.

compounds [42]. The O K-edge XANES is characterized by three features, denoted as A, B, and C in Fig. 2(c) at 530, 535, and 540 eV, respectively; and a small intensity prepeak denoted by an asterisk at 527 eV. The first structure (peak A in our case) is generally ascribed to the mixing between the transition metal d states with the O p states, thus giving information on the crystal field splitting of the $3d$ levels. In our data, this feature extends from 526 to 532 eV, and the fact that a single peak

is observed suggests a very small crystal field splitting (a fit of this peak with two different Lorentzian functions yields a splitting lower than 0.5 eV between them). By comparison to the O K edge XANES of other related iron oxides like FeO (Fe^{2+}), Fe_3O_4 ($Fe^{2.5+}$), and $\alpha-Fe_2O_3$ (Fe^{3+}) [52], we note that this first structure appears always at approximately the same energies independently of the iron valence, in clear contradiction with the interpretation given by Ko *et al.* [27], which implies the assignment of peaks A and B to the mixing of O p states with the Fe^{+3} and Fe^{+2} d states, respectively.

With the purpose of determining the electronic and structural origin of the different features in the O K-edge XANES spectra, we have carried out theoretical simulations in the frame of MS theory using the FDMNES code [49]. The MS calculations were performed by increasing the dimension of the atomic clusters around the absorber oxygen atoms and using the high temperature hexagonal cell of $LuFe_2O_4$ [9]. We have separately calculated the cross section for each of the two nonequivalent oxygen atoms O1(6c) and O2(6c) since they show different bond distance distributions. Figures 3(a) and 3(b), respectively, show the simulations for each oxygen atom, using various cluster sizes. O1 corresponds to the oxygen inside the Fe-O bilayer coordinated in the first shell to the Fe atoms, whereas O2 is in the Lu-O layer mainly coordinated to the Lu atoms. The simulations as a function of the cluster dimension show several results. Starting from the lower energy side, the first prepeak at 527 eV comes out in the simulation for O2 when the three Lu nearest neighbors (NNs) are included in the cluster, indicating that it is originated by the hybridization between the O $2p$ and Lu $5d$ orbitals. On the other hand, the main contribution to peak A ($\sim$529 eV) comes from the O1 atom, illustrating the origin in the mixing between the O $2p$ and Fe $3d$ states. This peak evolves from one resonance, when only the three Fe NNs are included in the cluster, to two resonances, when the FeO_5 bipyramids are completed in a similar way, as reported for the case of Fe in octahedral coordination [53]. Last, the B and C features are similar for the two oxygen atoms and come from MS contributions in coordination shells beyond 2.3 Å. In this way, peak A is successfully explained in terms of the O $2p-$Fe $3d$ hybridization without taking into account the valence states of the Fe atoms, while peak B originates from MS contributions of atoms beyond the first Fe coordination shell. Finally, in Fig. 3(c) are shown the average theoretical polarized and unpolarized spectra for a cluster of 4.5 Å obtained from the addition of the corresponding simulations for the two oxygen atoms. For this particular cluster size, the simulation converges for both O1 and O2 (this can be concluded by comparison with larger cluster sizes calculations but they are omitted in the figures for the sake of clarity). The *, A, B, and C spectral features are labeled in agreement with the experimental data. Although there is some discrepancy in the relative intensity, the agreement between theory and experiment is reasonable, and the spectral features and their separation in energy are well reproduced. We would like to note that when the Lu atoms in the structure are replaced by Y atoms [see inset of Fig. 3(c)], the prepeak * is no longer present, and the B and C features shift to lower energy, in agreement with the experimental data of YFe_2O_4.
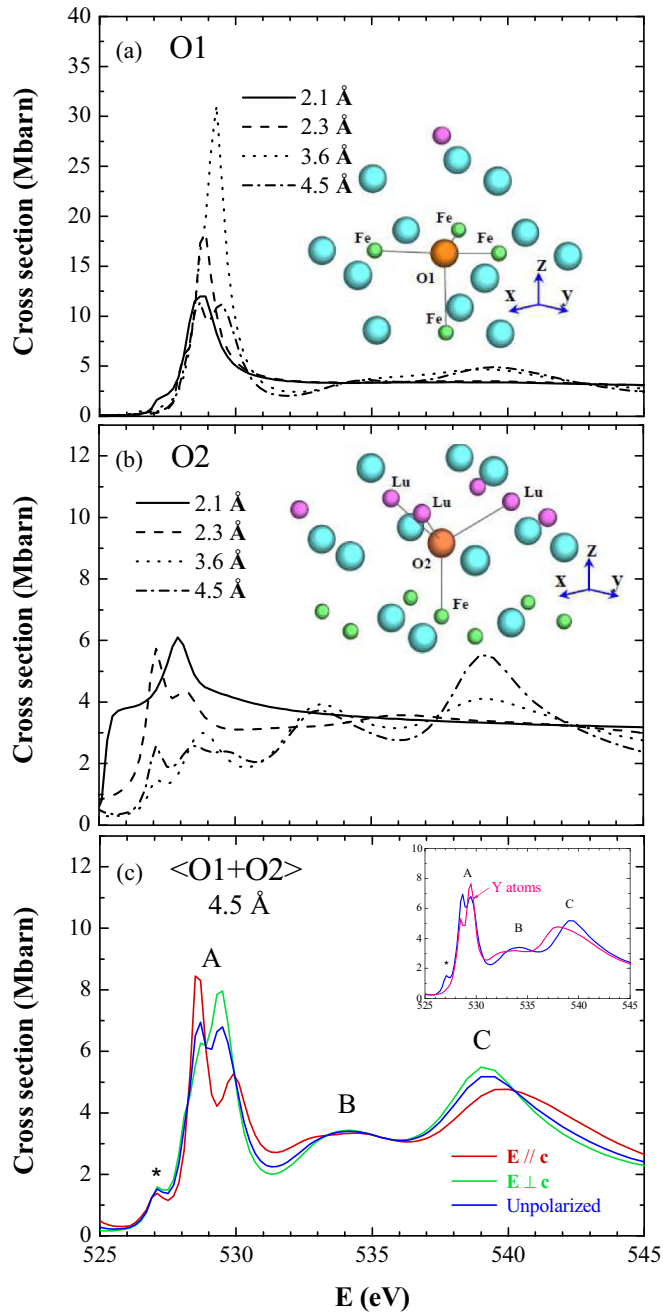
FIG. 3. (Color online) MS theoretical calculations at the O K edge using the hexagonal structure of LuFe$_2$O$_4$. Panels (a) and (b) show the evolution with increasing cluster radius around O1 and O2 sites, respectively. A picture of representative clusters (up to 3.6 Å for O1 and 4.1 Å for O2) is included in both cases, where the Lu, Fe, and O atoms are represented by pink, green, and blue spheres, respectively. The absorber O atom in each case is marked in orange, and the solid lines indicate the bonds to the nearest neighbors. (c) Comparison between the polarized and unpolarized calculated XANES spectra after addition of the O1 and O2 contributions for a cluster radius of 4.5 Å. Inset: The same unpolarized calculated spectrum compared to an equivalent calculation by replacing the Lu atoms with Y atoms.

B. XANES at the Fe $L_{2,3}$ edges

Figure 4(a) compares the spectra of mixed-valence RFe$_2$O$_4$ (R = Lu, Yb, Tm, Y) and LuFeCoO$_4$ polycrystals, while
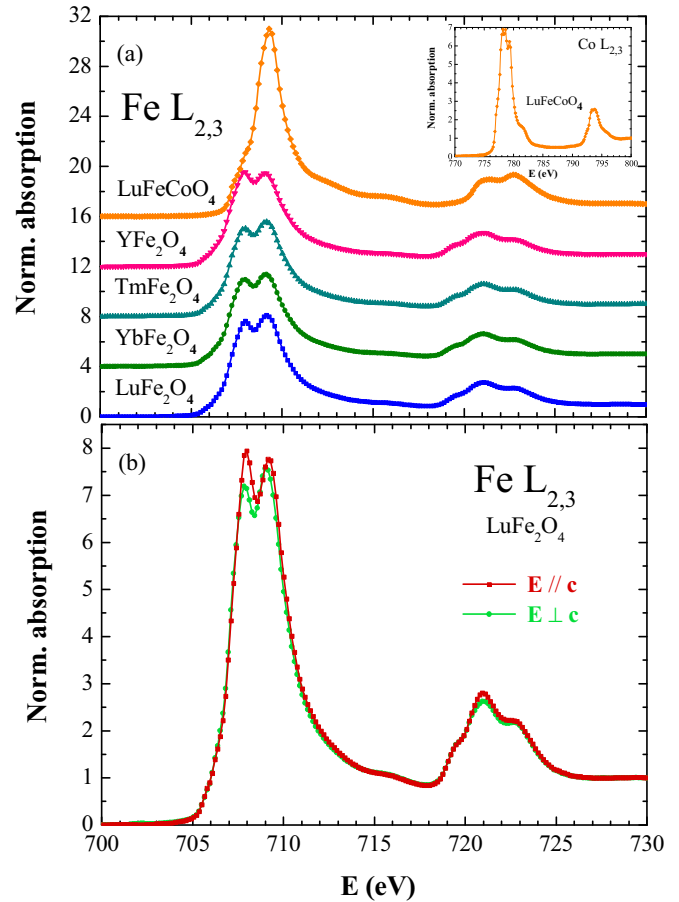

FIG. 4. (Color online) Normalized XANES spectra at the Fe $L_{2,3}$ edges measured by TEY at room temperature. (a) Spectra for the RFe$_2$O$_4$ (R = Lu, Yb, Tm, and Y) and LuFeCoO$_4$ polycrystalline samples shifted in vertical for the sake of comparison. Inset: Normalized XANES spectrum at the Co $L_{2,3}$ edges measured by TEY at room temperature for LuFeCoO$_4$. (b) Polarized XANES spectra for the LuFe$_2$O$_4$ single crystal.

Fig. 4(b) shows the polarized spectra $\mathbf{E}$ // $\mathbf{c}$ and $\mathbf{E}$ $\perp$ $\mathbf{c}$ for the LuFe$_2$O$_4$ single crystal. The XANES spectra at the Fe $L_{2,3}$ edges of the RFe$_2$O$_4$ series are very similar to each other, showing a minimum influence of the type of R^{+3}. On the contrary, the XANES spectrum of LuFeCoO$_4$ is markedly different, and its line shape is very similar to that shown by iron oxides with formal valence Fe^{+3} like LaFeO$_3$ [54] and α-Fe$_2$O$_3$ [55]. Besides, the XANES of LuFeCoO$_4$ at the Co $L_{2,3}$ edges agrees with that of compounds with formal valence Co^{2+} [56]. On the other hand, the major difference in the XANES at the Fe $L_{2,3}$ edges between $\mathbf{E}$ // $\mathbf{c}$ and $\mathbf{E}$ $\perp$ $\mathbf{c}$ is a small change in the relative intensity of the two peaks at the white line. Therefore, the electronic anisotropy is weak, as seen above for the O K edge and previously reported at the Fe K edge [42].

In order to get further information on the Fe valence state in the RFe$_2$O$_4$ compounds, we have evaluated the spectra of LuFe$_2$O$_4$ in terms of a 1:1 addition of the spectra corresponding to formal states Fe^{+2} and Fe^{+3}, respectively. Regrettably, only the experimental data corresponding to the Fe^{+3} formal valence (i.e., μ_{LuFeCoO4}) was measured. Therefore,
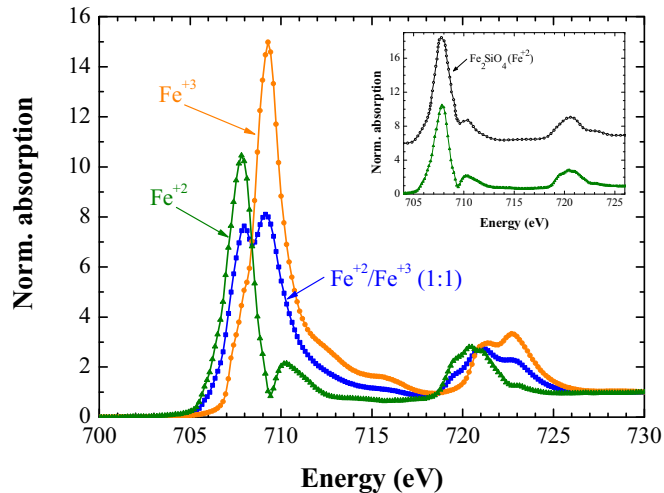
FIG. 5. (Color online) Normalized XANES spectra of a $LuFe_2O_4$ polycrystal ($\mu_{LuFe_2O_4}$) at the Fe $L_{2,3}$ edges measured by TEY at room temperature together with the contributions of Fe^{+3} (corresponding to the absorption of a $LuFeCoO_4$ polycrystal, $\mu_{LuFeCoO_4}$) and Fe^{+2} (corresponding to $2\mu_{LuFe_2O_4} - \mu_{LuFeCoO_4}$) in a ratio 1:1. Inset: Comparison between our Fe^{+2}-XANES spectrum and the XANES data measured for Fe_2SiO_4 with Fe^{+2} formal valence state taken from Ref. [49].

in order to overcome this problem and check whether the $LuFe_2O_4$ spectrum agrees with the 1:1 addition of the Fe^{+2} and Fe^{+3} spectra, we have evaluated the weighted difference between $\mu_{LuFe_2O_4}$ and $\mu_{LuFeCoO_4}$ as representative of Fe^{+2} formal valence. Figure 5 compares the XANES spectrum of $LuFe_2O_4$ to those spectra corresponding to Fe^{+3} and Fe^{+2}. The so-obtained Fe^{+2} spectrum agrees very well with the XANES of Fe_2SiO_4 with formal valence Fe^{+2} [57] (see inset of Fig. 5), thus corroborating the description of the Fe valence state in $LuFe_2O_4$ as a mix Fe^{+2}/Fe^{+3} in a ratio 1:1. Moreover, we have also validated this description by the theoretical calculations of the XANES spectra corresponding to Fe^{+2} and Fe^{+3} in bipyramidal configuration obtained with the CTM4XAS code [51] (not shown here). Strikingly, the description of the Fe valence state in $LuFe_2O_4$ in terms of Fe^{+3} and Fe^{+2} pure ionic species seems to contradict the results obtained using other techniques. High resolution synchrotron powder diffraction and RXS [10,43,44] experiments have shown that the single Fe crystallographic site in the symmetric hexagonal phase at high temperature splits into several different sites in the distorted phases at low temperatures in which the charge segregation is very small (below 0.5 electrons) and multimodal. Besides, the XANES spectra at the Fe K edge [42] and O K edge cannot be reproduced by the weighted addition of Fe^{+3} and Fe^{+2} representative spectra. However, all the results can be reconciled by describing the Fe formal mixed-valence state within a configuration interaction model for the d states as follows. In the hexagonal phase, each Fe atom is in a fractional state $3d^{5.5}$, corresponding to the addition of the mixed configurations $0.5\,3d^5 + 0.5\,3d^6$, and in the distorted phases the $3d$ population remains the same in average but there are different mixtures $\alpha\,3d^5 + \beta\,3d^6$ with $\alpha + \beta = 1$ for each Fe atom with noninteger valence. We note that

this configuration interaction model would only apply to the localized $3d$ states and therefore is not at conflict with the results obtained at the Fe K edge where highly delocalized $4p$ states are probed.

Prior to concluding this section, we would like to make some comments. First, the spectral shape of the XANES spectra for the $LuFe_2O_4$ polycrystalline samples with either polished or cleaved surfaces barely varies (not shown here). Second, the XANES spectra measured by FY detection are highly distorted due to SA, which is particularly relevant at the intense Fe $L_{2,3}$ white lines. After correcting for SA, the spectra recorded in FY are nearly identical to those recorded in TEY (see the Appendix). As will be discussed later, these agreements assure us that the same electronic structure is measured in both the polished and cleaved samples by means of either TEY or FY.

C. XMCD at the Fe $L_{2,3}$ edges

The XMCD spectra at the Fe $L_{2,3}$ edges of the RFe_2O_4 samples (R = Lu, Yb, Tm) were measured with $H = 4$ T at different temperatures in the range 260–150 K depending on the sample. Both TEY and FY detection methods were simultaneously used. We note that the TEY detection is limited at low temperature because the samples are too insulating and a charging effect is produced after the photoelectric absorption process. Figure 6 shows the XMCD spectra recorded in TEY for the $LuFe_2O_4$ single crystal and RFe_2O_4 (R = Lu, Yb, Tm) polycrystalline samples as a function of temperature. The $LuFe_2O_4{}^*$ label refers to the sample with cleaved surface (for all the others the surface was polished). The spectral shape of the XMCD signal is very similar among the different samples and agrees with previous reports in the literature [27,30,38]. On the other hand, the magnitude of the XMCD signal for each sample increases upon cooling down in temperature, in agreement with the macroscopic magnetization (see Fig. 1). The strong difference in the magnitude of the dichroic signal between the two configurations **H // c** and **H ⊥ c** obtained in the $LuFe_2O_4$ single crystal also agrees with the strong macroscopic magnetic anisotropy of this material [see Fig. 1(d)]. Moreover, the magnitude of the XMCD signal of the three RFe_2O_4 (R = Lu, Yb, Tm) polycrystalline samples at 200 K is very similar in accordance with their close macroscopic magnetization value at this temperature [see Figs. 1(a)–1(c)]. It is noteworthy that the XMCD signal for the $LuFe_2O_4{}^*$ cleaved sample is about 2.5 times larger than the one of the $LuFe_2O_4$ polished sample [compare Fig. 6(c) to Fig. 6(d)]. Given that the corresponding XANES spectra are alike between cleaved and polished samples, this result is likely to be due to differences in the magnitude of the magnetic moment between the two samples. However, the macroscopic magnetization was checked to be the same for both of them (not shown here); therefore, the most likely scenario is a reduction of the magnetic moment at the surface. This phenomenon is also found in at least the three following archetypical magnets: Fe, Ni, and Fe_3O_4. On one hand, the dichroic signal of Fe and Ni measured by TEY in the pioneer XMCD experiment by Sette *et al.* [58] is several times smaller than the corresponding signal recorded in transmission [59]. On the other hand, the intensity of the XMCD spectrum of Fe_3O_4 recorded in TEY
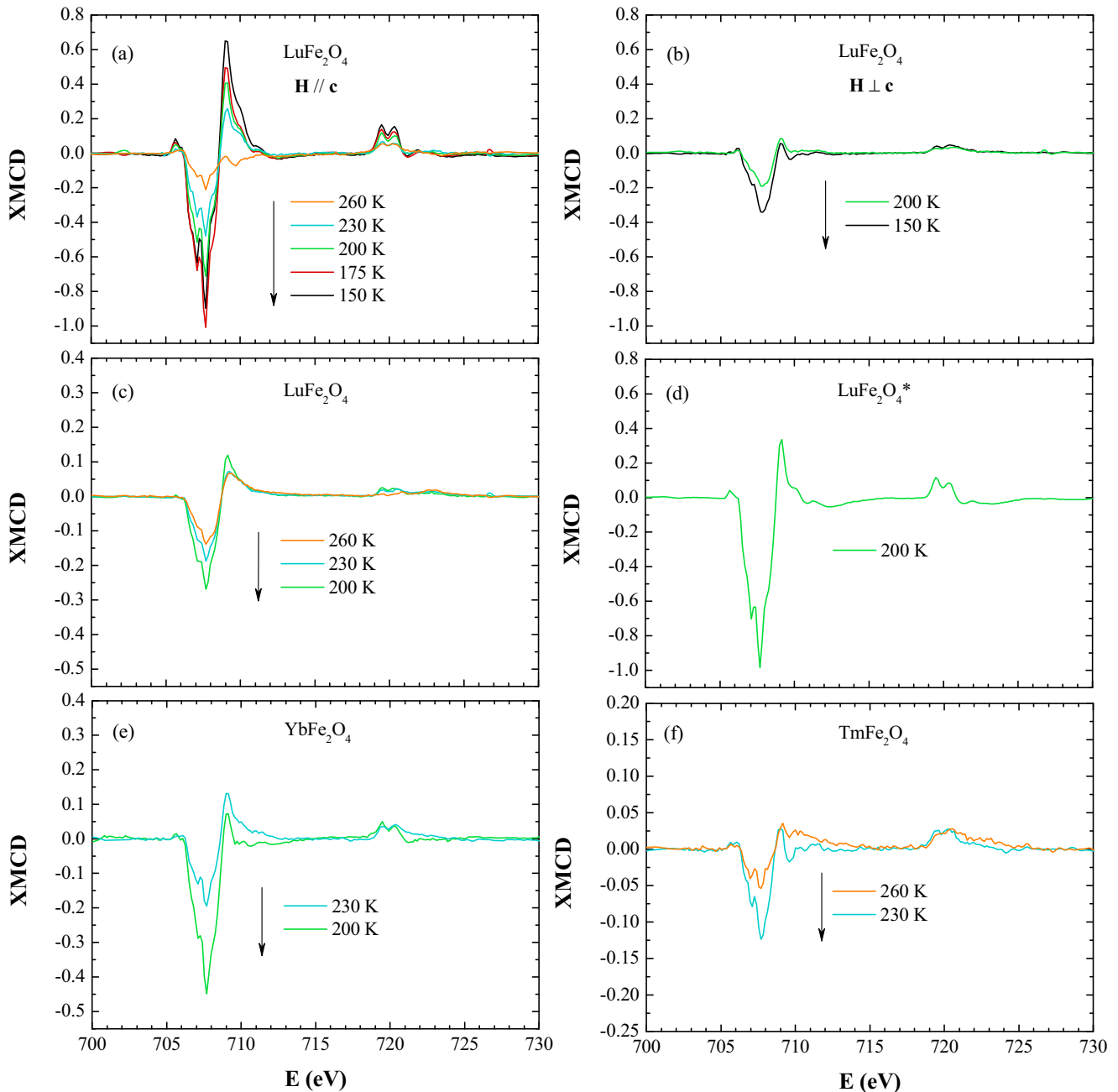
FIG. 6. (Color online) XMCD spectra at the Fe $L_{2,3}$ edges measured by TEY with a magnetic field of 4 T as a function of temperature for (a) LuFe$_2$O$_4$ single crystal with **H** // **c,** (b) LuFe$_2$O$_4$ single crystal with **H** $\perp$ **c**, (c) LuFe$_2$O$_4$ polycrystal, (d) LuFe$_2$O$_4$* polycrystal, (e) YbFe$_2$O$_4$ polycrystal, and (f) TmFe$_2$O$_4$ polycrystal. All the samples were polished *in situ* except for the LuFe$_2$O$_4$* sample that was cleaved.

is very small too [60], and it has also been reported a decrease by a factor of two in the XMCD signal measured by TEY of a polished magnetite crystal with respect to a cleaved crystal measured under the same conditions [61].

Since the TEY absorption detection method probes mainly the surface of the material (the sampling depth is of the order of a few nanometers according to the electron mean free path at these energies), we could explain the differences between the two surface preparation processes as due to the larger surface contribution of the polished sample in comparison with the cleaved one. In order to confirm this hypothesis, we have also evaluated the XMCD spectrum of the cleaved sample

LuFe$_2$O$_4$* recorded in FY. The XANES spectra for right and left circular polarized light were corrected for SA using the method given in the Appendix. As shown in the Appendix, the SA-corrected FY-detected XANES at the Fe L_3 and L_2 edges perfectly fit to the corresponding TEY data, demonstrating the adequacy of the proposed method and that the spectra recorded in TEY probe the same electronic structure as FY. That is to say, the agreement between the TEY and SA-corrected FY XANES spectra at the Fe $L_{2,3}$ for both polished and cleaved samples ensures that we can discard any surface contamination. Figure 7 compares the XMCD spectra for the LuFe$_2$O$_4$* cleaved sample measured by TEY and FY after correcting
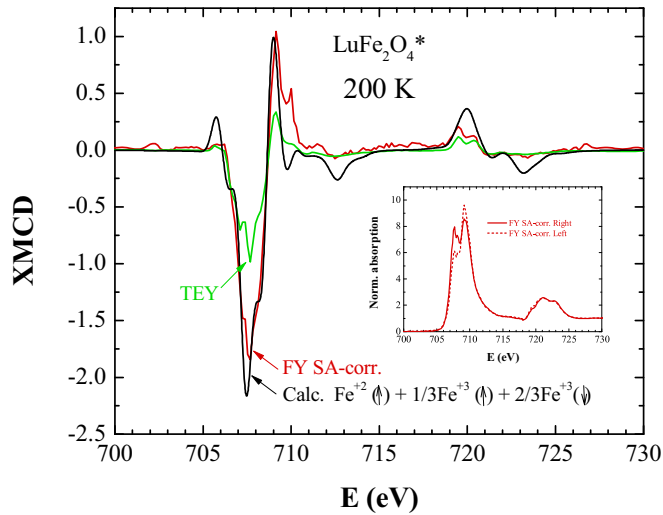
FIG. 7. (Color online) Fe $L_{2,3}$ edge XMCD spectra of the LuFe$_2$O$_4$* sample at 200 K. The dichroic spectra measured by TEY and FY SA-corrected is compared to the corresponding theoretical simulation obtained by multiplet calculations using the spin ordering model indicated in the figure. Inset: Normalized XANES spectra in FY SA-corrected measured with right and left helicity at 200 K.

for SA. The TEY and SA-corrected FY XMCD spectra are very similar except for their magnitude: the SA-corrected FY spectrum is about two times more intense. In summary, our results imply that the intensity of the XMCD signal increases as the surface contribution decreases ($I_{\mathrm{XMCD,TEY,polished}} < I_{\mathrm{XMCD,TEY,cleaved}} < I_{\mathrm{XMCD,FY,cleaved}}$), while its shape remains unaltered. This behavior can only be explained if we assume that the magnetization decreases when going from the bulk to the surface. Obviously, it would be necessary to carry out specific experiments in order to quantify this effect.

As we concluded in Sec. III B, the XANES spectra at the Fe $L_{2,3}$ edges of RFe$_2$O$_4$ are well described by the addition of the two electronic configurations $3d^5/3d^6$, which can be alternatively defined as Fe^{+3}/Fe^{+2} contributions. The XMCD spectrum at the L_3 edge shows for all the samples a strong negative signal at the energy position of the Fe^{+2} contribution, whereas a weaker positive signal is obtained at the energies of the Fe^{+3} contribution, indicating an antiferromagnetic ordering between the two ions/configurations. In order to quantify these two contributions, we have assumed a simple approach considering that the dichroic signal of each component is proportional to the respective absorption signal (positive for Fe^{+3} and negative for Fe^{+2}). Under this assumption, the XMCD spectra of all the samples at the different measured temperatures were fitted by using the absorption contributions of Fe^{+3} and Fe^{+2} with the appropriate sign. We obtained a qualitatively good agreement with a Fe^{+3}/Fe^{+2} ratio for the two contributions to the XMCD signal ranging between 0.25 and 0.45, being the average ratio equal to 0.33. This ratio 1:3 for the Fe^{+3} and Fe^{+2} contributions agrees with the ferrimagnetic spin ordering already proposed [27,30,37,38], in which all the Fe^{+2} spins and 1/3 of the Fe^{+3} spins are ordered ferromagnetically whereas the remaining 2/3 of the Fe^{+3} spins order antiferromagnetically. The simulation corresponding to this spin ordering model obtained by multiplet calculations
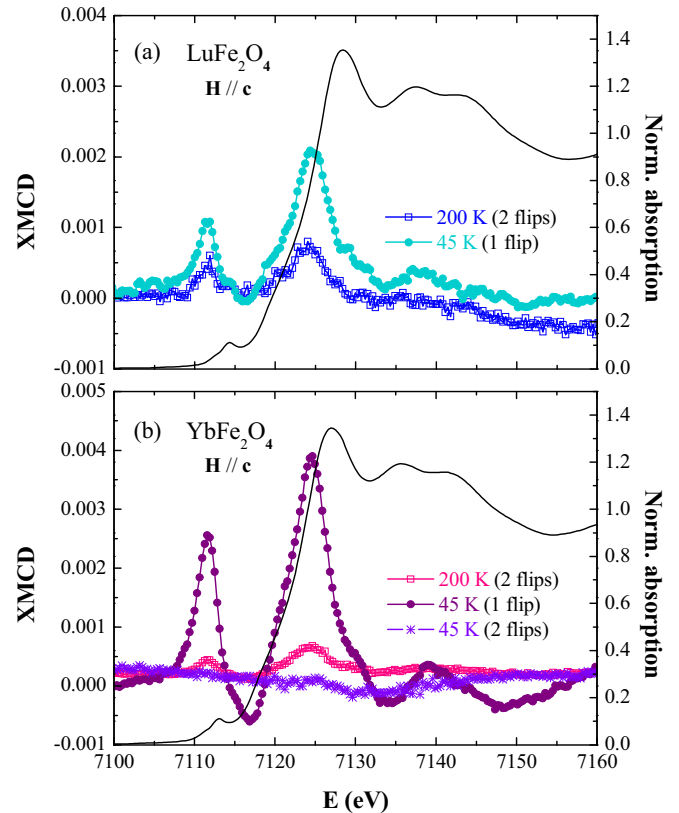

FIG. 8. (Color online) XMCD (left axis) and XANES (right axis) spectra at the Fe K edge measured for (a) LuFe$_2$O$_4$ and (b) YbFe$_2$O$_4$ polycrystalline oriented samples with an applied magnetic field $\mathbf{H} \approx$ 1 T parallel to the c axis.

is also compared in Fig. 7 with the XMCD results for the LuFe$_2$O$_4$* cleaved sample. Since the experimental data were measured at 200 K, the theoretical simulation obtained for 0 K has been renormalized by the relationship between the macroscopic magnetizations $M_{T=200\,\mathrm{K}}/M_{T=0\,\mathrm{K}} \approx 0.5$ (see Fig. 1) for a direct comparison. As can be seen, the shape and magnitude of the theoretical simulation corresponding to the spin ordering Fe^{+2}($\uparrow$) + 1/3Fe^{+3}($\uparrow$) + 2/3Fe^{+3}($\downarrow$) agrees rather well with the SA-corrected FY XMCD signal. This fact reinforces the hypothesis that the XMCD$_{\mathrm{FY,cleaved}}$ represents the bulk magnetization, whereas the XMCD$_{\mathrm{TEY,cleaved}}$ reflects the decrease of the magnetization near the surface.

D. XMCD at the Fe K edge

Figure 8 shows the XMCD spectra at the Fe K edge of oriented powder RFe$_2$O$_4$ samples (R = Lu, Yb) with $H \approx$ 1 T applied along the c axis direction at 45 and 200 K. At 200 K, the four symmetry cases of the XMCD signal, obtained by flipping the helicity of the incoming photons (right/left) and the magnetic field ($\uparrow/\downarrow$), have been recorded. The XMCD signals are then calculated independently for the two polarization cases, flipping the magnetic field, and averaged. Hereafter, this method will be referred to as two flips. On the other hand, since the coercive field at low temperatures for the RFe$_2$O$_4$ (R = Lu, Yb) compounds is well above $H \approx$ 1 T, an alternative method of only flipping the helicity of the incoming

photons first for positive **H** and then for negative **H** was used at 45 K, which will be referred to as one flip. Furthermore, in order to enhance the XMCD signal at low temperatures, a field-cooling (FC) process was performed starting from temperatures above T_N. The XMCD spectrum is similar for both samples and shows one positive peak between 7108 eV and 7114 eV (pre-edge), followed by a small peak with opposite sign located between 7114 eV and 7119 eV. From 7119 eV up to 7132 eV (absorption edge), a rather broad feature appears with a positive sign. The magnitude of these XMCD signals nicely agrees with the temperature dependence of the macroscopic magnetization ($M_{FC, T=45 K} > M_{T=200 K}$) for both compounds (see Fig. 1). Moreover, in Fig. 8 it can be corroborated that the XMCD signal is nearly zero at 45 K when it is measured with the two-flips method as expected, since **H** is not large enough to reverse the magnetization due to the huge coercive field of the sample. The XMCD pre-edge feature stems from the lack of inversion center of the bipyramid local symmetry at the Fe site, which allows the Fe $3d$-$4p$ hybridization.

IV. DISCUSSION AND CONCLUSIONS

In this paper, the electronic and magnetic structure of the RFe$_2$O$_4$ family was studied by means of soft XAS and XMCD measurements, with emphasis in LuFe$_2$O$_4$. This investigation adds to other recent published papers [10,38–44] to provide a framework for the physics of the mixed-valence RFe$_2$O$_4$ (R = Lu, Yb, Tm, Y) compounds, which in some aspects can be extended to other mixed-valence oxides. In this framework, the Fe atoms are in a homogenous mixed-valence state at temperatures both above and below the so-called CO transition. In the symmetric hexagonal phase ($T > T_{CO}$), there is only one crystallographic site for Fe; therefore, the formal valence is Fe$^{+2.5}$, as deduced from the stoichiometry. Upon cooling down ($T < T_{CO}$), LuFe$_2$O$_4$ undergoes two structural transitions that reduce the crystal symmetry to successive monoclinic and triclinic symmetries at about 320 K and 200 K, respectively [10,43]. The single crystallographic site in the hexagonal cell splits into four and six nonequivalent sites in the monoclinic $C2/m$ and triclinic $P\bar{1}$ cells, respectively, implying four-modal and trimodal valence distributions in which the maximum charge segregation is below 0.5 electrons [44]. In this case, each Fe atom is in a homogeneous mixed-valence state whose formal valence can be described by Fe$^{+2.5\pm\delta}$ with $\delta < 0.25$. Similar crystal distortions are likely to occur in YFe$_2$O$_4$, whereas the YbFe$_2$O$_4$ and TmFe$_2$O$_4$ compounds maintain the hexagonal crystal symmetry down to 80 K and their distortions remain disordered [10].

As shown in our results, XANES spectra at the O K edge are very similar for the RFe$_2$O$_4$ (R = Lu, Yb, Tm) compounds and the reference LuFeCoO$_4$ with formal valence Fe^{+3}. This result demonstrates that the O p-projected density of states is not very sensitive to either the Fe valence state or the type of rare earth. Slight differences between the spectrum of the Y-compound and all the others have been identified as a trace of the Y $4d$ states in the XANES at the O K edge. The spectrum of LuFe$_2$O$_4$ is well described by simulations based in the MS theory [see Fig. 2(c)], which have shown that the prepeak * and peak A come from the hybridization between O $2p$ and Lu $5d$

and Fe $3d$ states, respectively, whereas peaks B and C come from MS contributions of atoms beyond the first coordination shell.

The XANES spectra at the Fe $L_{2,3}$ edges are nearly equal for all the members of the series. By comparison with the LuFeCoO$_4$ spectrum, we have found that the spectrum of LuFe$_2$O$_4$ agrees with the addition of Fe^{+3} and Fe^{+2} representative spectra in a 1:1 ratio, suggesting the presence of either two iron valences or two atomic configurations. Due to the fact that these spectra are independent of the temperature (they do not change across the different crystallographic phases) and also of the kind of R atom, we can conclude that the d states for the mixed-valence Fe ion in RFe$_2$O$_4$ can be described as a mixture of $3d^5$ and $3d^6$ configurations. Therefore, within a configuration interaction framework, the electronic state can be represented in the hexagonal phase by the addition $0.5\,3d^5 + 0.5\,3d^6$ and in the low temperatures phases as $3d^{5+x} = x\,3d^6 + (1-x)\,3d^5$. This description is consistent with the magnetic susceptibility of LuFe$_2$O$_4$ in the paramagnetic phase [37] where the magnetic moment corresponds to $3d^{5.5}$ occupation.

In the same way, the theoretical analysis of the XMCD spectra at the Fe $L_{2,3}$ edges using multiplet calculations agrees with the ferrimagnetic spin ordering Fe$^{+2}(\uparrow) + 1/3$Fe$^{+3}(\uparrow) + 2/3$Fe$^{+3}(\downarrow)$ that is generally proposed for LuFe$_2$O$_4$ [27,30,37,38]. By considering the simple ionic limit ($4\,\mu_B$ for Fe^{+2} and $5\,\mu_B$ for Fe^{+3}), this $2(\uparrow) : 1(\downarrow)$ spin alignment, however, yields a total spin magnetic moment of $2.33\,\mu_B$/f.u., which is much lower than the experimental saturation magnetization value $M_S \approx 2.8\,\mu_B$/f.u. along the easy magnetic axis at 4 K [see Fig. 1(d)]. The experimental M_S better agrees with the above ferrimagnetic spin ordering if the magnetic moment of each Fe ion is taken as $4.5\,\mu_B$ (corresponding to Fe$^{+2.5}$), which predicts $3\,\mu_B$/f.u. However, it has been argued that the large difference between the net spin moment and the saturation magnetization in the former model Fe$^{+2}(\uparrow) + 1/3$Fe$^{+3}(\uparrow) + 2/3$Fe$^{+3}(\downarrow)$ can be explained by an important orbital contribution from Fe^{2+} to the magnetization, which is generally quenched by the crystal field. To explore the orbital magnetic moment, several works [27,30,38] have applied the sum rules to the XMCD spectrum of LuFe$_2$O$_4$, concluding on the existence of a large orbital component that may also explain the strong magnetic anisotropy of this material. We have also performed this analysis for all the samples (even when the magnetization is strongly reduced by surface effects), and we find values for the ratio between the orbital and spin moments m_o/m_s ranging between 0.3 and 0.5, similar to what has been previously reported (0.34 [27], 0.7 [30], and 0.3 [38]). In order to verify the applicability of these sum rules to LuFe$_2$O$_4$, we have applied them to each of the theoretical Fe^{+3} and Fe^{+2} calculated XMCD spectra. The m_o and m_s values obtained are $0.9\,\mu_B$ and $2.62\,\mu_B$ for Fe^{+2} and $0\,\mu_B$ and $3.32\,\mu_B$ for Fe^{+3}, respectively. In the two ionic cases, the obtained values differ considerably from the theoretical expected spin values, $m_s = 4\,\mu_B$ and $m_s = 5\,\mu_B$ for Fe^{+2} ($3d^6$) and Fe^{+3} ($3d^5$) atoms, respectively. The errors estimated are about 40%, within the values admitted for $3d^5$ and $3d^6$ ions in solid state systems [50]. Taking into account this remark and the fact that the intensity of the XMCD signal for LuFe$_2$O$_4$ strongly depends on both the sample
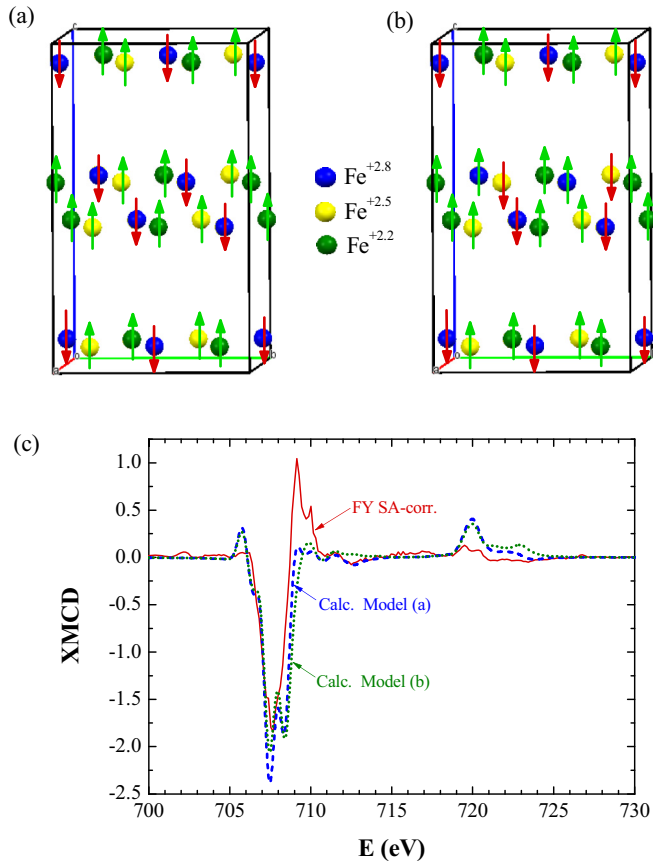
FIG. 9. (Color online) Top: Spin structures in $C2/m$ cell of the (a) $2/3[Fe_4^{+2.2}(\uparrow) + Fe_{31}^{+2.2}(\uparrow)] + 2/3[Fe_{32}^{+2.5}(\uparrow) + Fe_{22}^{+2.5}(\uparrow)] + 2/3[Fe_1^{+2.8}(\downarrow) + Fe_{21}^{+2.8}(\downarrow)]$ and (b) $2/3[Fe_4^{+2.2}(\uparrow) + Fe_{31}^{+2.2}(\uparrow)] + 2/3[Fe_{32}^{+2.5}(\uparrow) + 1/2Fe_{22}^{+2.5}(\uparrow) + 1/2Fe_{22}^{+2.5}(\downarrow)] + 2/3[Fe_1^{+2.8}(\downarrow) + 1/2Fe_{21}^{+2.8}(\downarrow) + 1/2Fe_{21}^{+2.8}(\uparrow)]$ models described in the text. Bottom: Theoretical simulations of the XMCD spectra for the two spin structures corresponding to models (a) and (b) compared to the FY SA-corrected XMCD experimental spectrum.

surface preparation and detection method ($I_{XMCD,FY,cleaved} \approx 2 I_{XMCD,TEY,cleaved} \approx 5 I_{XMCD,TEY,polished}$), we consider that the individual orbital and spin sum rules could not provide any reliable information on the orbital and spin components of the Fe magnetic moment in the case of $LuFe_2O_4$. In spite of this, the above Fe $L_{2,3}$ XMCD results seem to verify the full 2+/3+ valence separation, in clear contradiction to XAS [42] and RXS [43,44] results at the Fe K edge.

To address this question, we have analyzed the Fe $L_{2,3}$ XMCD spectra on the basis of the trimodal Fe valence distribution deduced for temperatures below T_N [43,44]. We have checked an alternative ferrimagnetic spin ordering model based on the assumption that Fe atoms with the same valence state (and crystallographic site) are always coupled ferromagnetically. The resulting spin ordering, shown in Fig. 9(a), is $2/3[Fe_4^{+2.2}(\uparrow) + Fe_{31}^{+2.2}(\uparrow)] + 2/3[Fe_{32}^{+2.5}(\uparrow) + Fe_{22}^{+2.5}(\uparrow)] + 2/3[Fe_1^{+2.8}(\downarrow) + Fe_{21}^{+2.8}(\downarrow)]$. This alternative model provides a similar spin-only contribution of $2.6\,\mu_B$/f.u. to the magnetic moment. The XMCD spectra for this spin structure was simulated within the configuration interaction framework, where $Fe^{+2.2}$ is a $3d^{5.8} =$

$0.8\,3d^6 + 0.2\,3d^5$ with $m_s = 4.2\,\mu_B$, $Fe^{+2.5}$ is a $3d^{5.5} = 0.5\,3d^6 + 0.5\,3d^5$ with $m_s = 4.5\,\mu_B$, and $Fe^{+2.8}$ is a $3d^{5.2} = 0.2\,3d^6 + 0.8\,3d^5$ with $m_s = 4.8\,\mu_B$; the resulting multiplet calculation is plotted in Fig. 9(c). For comparison, the high-field spin structure proposed by de Groot *et al.* [37] that best described the neutron diffraction data is shown in Fig. 9(b). It almost corresponds to our spin ordering model except that the spins of the crystallographic Fe_{21} and Fe_{22} sites in the Fe-O layer with $z = 0.57$ flip their sign, leading to an antiferromagnetic configuration with those Fe_{21} and Fe_{22} sites in the $z = 0.43$ Fe-O layer. Thus, the resulting spin ordering is $2/3[Fe_4^{+2.2}(\uparrow) + Fe_{31}^{+2.2}(\uparrow)] + 2/3[Fe_{32}^{+2.5}(\uparrow) + 1/2Fe_{22}^{+2.5}(\uparrow) + 1/2Fe_{22}^{+2.5}(\downarrow)] + 2/3[Fe_1^{+2.8}(\downarrow) + 1/2Fe_{21}^{+2.8}(\downarrow) + 1/2Fe_{21}^{+2.8}(\uparrow)]$, whose calculated XMCD spectrum is also plotted in Fig. 9(c) for comparison. Our spin ordering model gives a slightly better agreement with the experiment regarding the smaller upward peak at 710 eV, which is underestimated by the two calculations. On the other hand, the spin ordering by de Groot *et al.* [37] gives better agreement with the observed magnetic reflections. Although both spin structures considering the trimodal Fe valence configuration show worse agreement with the experimental XMCD signal than the $2(\uparrow):1(\downarrow)$ spin structure considering the purely ionic bimodal $Fe^{2+} - Fe^{3+}$ configuration (see the comparisons in Fig. 9(c) and Fig. 7, respectively), any of them are the best solution to account for the structure refinement [10,43], XAS [42], RXS [43–44], magnetic [37], and XMCD data. Indeed, the Mössbauer study by Tanaka *et al.* [62] disclosed that Fe ions are not in purely 2+ or 3+ and reported that there exist three distinguishable Fe^{3+}-like and Fe^{2+}-like sites, in clear agreement with the six nonequivalent crystallographic sites found for the triclinic low temperature structure [10] and the fractional Fe valence distribution, either the approximated trimodal or the real six-modal one.

The existence of a magnetic dichroic signal at the transition metal K edge in ferro- or ferrimagnetic systems is generally ascribed to the presence of orbital magnetic moment contribution to the magnetization. Therefore, our XMCD measurements at the Fe K edge confirm a large unquenched orbital magnetic moment in the Fe atom for the RFe_2O_4 systems that can account for the discrepancy between the spin-only ferrimagnetic models and the experimental M_S. On the other hand, and opposite to the results of XMCD at the Fe $L_{2,3}$ edges, the XMCD signal at the Fe K edge does not show two components corresponding to the two $Fe^{+3}(3d^5)$ and $Fe^{+2}(3d^6)$ ions (configurations); therefore, the Fe p states cannot be described in terms of the 1:1 addition of the Fe^{+3} and Fe^{+2} contributions, in agreement with previous XAS measurements at the Fe K edge [42]. Otherwise, it could be consistent with the alternative ferrimagnetic-ordering model considering that $Fe^{+2.8}$ mostly contribute to the pre-edge feature.

It is noteworthy that for the other RFe_2O_4 ($R = $ Yb, Tm) compounds in which no charge disproportionation occurs down to 80 K [10], the XMCD spectra at the Fe $L_{2,3}$ edges are like the one of $LuFe_2O_4$ composed by two opposite signals that can be ascribed to Fe^{+3} ($3d^5$ configuration) and Fe^{+2} ($3d^6$ configuration).

As a final remark, the systematic XAS-XMCD study at the Fe $L_{2,3}$ edges in the same $LuFe_2O_4$ polycrystalline sample as a function of both the surface-cleaning process

(polished and cleaved) and detection method (TEY and FY) has evidenced new results related to the magnetic properties. The fact that all the XMCD spectra can be superimposed and only differ in magnitude in such a way that $I_{\text{XMCD,FY,cleaved}} \approx 2I_{\text{XMCD,TEY,cleaved}} \approx 5I_{\text{XMCD,TEY,polished}}$ while the corresponding XAS spectra are equivalent points to a reduced surface magnetization. This finding, which was also reported in the case of Fe$_3$O$_4$ [53], opens up the possibility of studying new interesting phenomena from the viewpoint of basic science and applications such as magnetization changes at the interfaces.

APPENDIX

1. Self-absorption (SA) correction

As it has been widely described in the literature, XANES spectra at the transition metal $L_{2,3}$ edges measured in FY for thick, concentrated samples are highly distorted by SA mainly at the strong white lines energies. *Ab initio* corrections are difficult since the parameters involved are not always well known and sometimes the theoretical models do not take into account all the experimental constraints. We propose here an empirical method to correct the SA in XANES spectra recorded by FY, which relies on the equivalent measurement recorded by TEY for the same sample and conditions. The method consists in fitting the XANES spectrum measured in FY to the corresponding spectrum measured in TEY, which is free of SA.

The apparent absorption coefficient measured in fluorescence in the case of samples that are thick with respect to the penetration depth of the photons is related to the real absorption coefficient $\mu(E)$ by [63]:

$$\mu'(E) = \frac{I_f}{I_0} = \frac{(\Omega/4\pi)\varepsilon_f \mu(E)}{\mu_T(E) + \mu_T(E_F)\frac{\sin\phi}{\sin\theta}}, \quad \text{(A1)}$$

where I_f and I_0 are the fluorescence and incoming flux intensities, $\mu_T(E)$ is the total absorption coefficient including contributions from the edge of interest and from other atoms and edges of the atom of interest ($\mu(E) + \mu_{\text{background}}(E)$), $\mu_T(E_F)$ is the total absorption coefficient at the energy of the fluorescence photons E_F, ϕ and θ are the angles between the sample surface and the direction of the incoming and the detected fluorescence photons, respectively, and $\Omega/4\pi$ and ε_f are the solid angle covered by the detector and the fluorescence yield of the absorber atom.

In our case, $\mu_T(E)$ can be approximated to $\mu_T(E) = \mu(E) + k$, where k is constant since the energy range at the Fe $L_{2,3}$ edges is small. Taking into account that the other terms in Eq. (A1) are also constants, we arrive at the expression,

$$\mu'(E) = \frac{A \cdot \mu(E)}{(\mu(E) + C)}, \quad \text{(A2)}$$

where A and C are parameters to take into account all the SA corrections. Therefore, $\mu(E)$ free of SA can be rewritten as follows:

$$\mu(E) = \frac{C \cdot \mu'(E)}{(A - \mu'(E))}. \quad \text{(A3)}$$

Using Eq. (A3), we have fitted the average XANES spectrum between the two circular polarization measurements recorded in FY ($\mu'(E)$) to the corresponding spectrum recorded in TEY after subtracting the background ($\mu(E)$). This procedure has been applied for the L_3 and L_2 edges separately. Figure 10 illustrates the comparison between the pre-edge subtracted TEY data and the fit obtained for the FY-detected XANES spectrum of the LuFe$_2$O$_4$* cleaved sample at 200 K. As it can be seen, the agreement between the TEY-detected XANES spectrum and the fit (i.e., the SA-corrected FY-detected XANES spectrum) is very good, showing that the spectra are nearly identical for the two detection methods. In order to correct for SA the XMCD spectra measured in FY, the following procedure was applied.
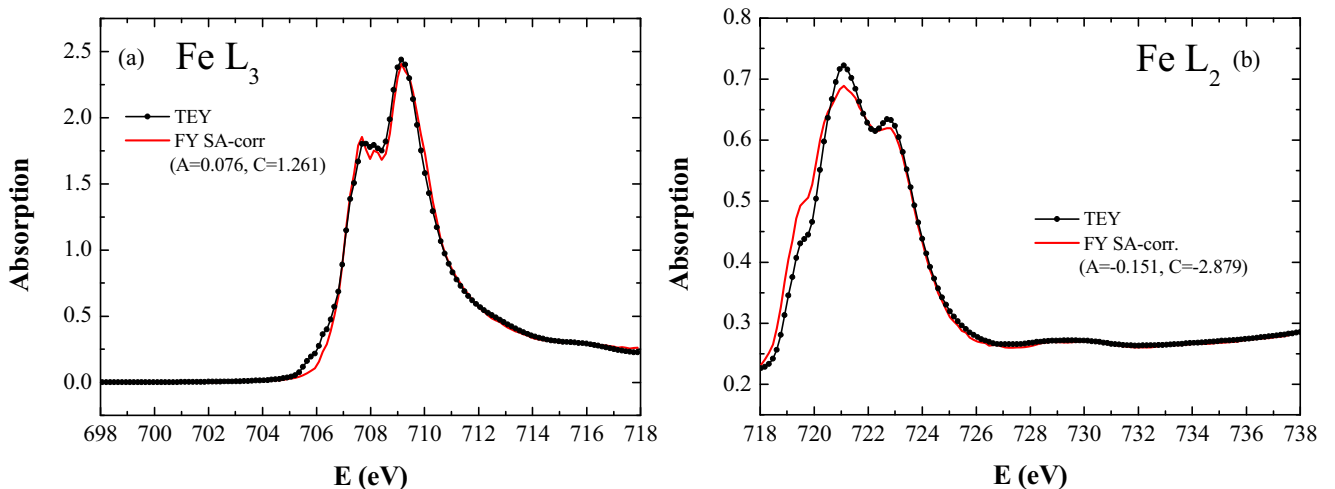

FIG. 10. (Color online) Comparison between the XANES spectra at the Fe L_3 edge (a) and L_2 edge (b) for the LuFe$_2$O$_4$* sample at 200 K measured by TEY and FY after correcting for self-absorption (SA) using the SA-correction method described in the Appendix.

First, each XANES spectrum $\mu^+(E)$ (right-handed circular polarization) and $\mu^-(E)$ (left-handed circular polarization) were corrected separately applying Eq. (A3) and using the A and C parameters resulting from the fit of the average XANES spectrum. Second, the SA-corrected FY XMCD was obtained by subtracting the SA-corrected $\mu^+(E)$ and $\mu^-(E)$ spectra. The resulted XMCD as well as the μ^+ and μ^- results can be seen in Fig. 7 of the paper for the $LuFe_2O_4$* cleaved sample.

[1] S. Maekawa, T. Tohyama, S. E. Barnes, S. Ishihara, W. Koshibae, and G. Khaliullin, *Physics of Transition Metal Oxides*, Springer Series in Solid State Science, Vol. 144 (Springer-Verlag, Berlin Heidelberg, 2004).

[2] S. W. Cheong and M. Mostovoy, Nat. Mater. **6**, 13 (2007).

[3] N. Kimizuka, Y. Takenaka, Y. Sasada, and T. Katsura, Solid State. Commun. **15**, 1321 (1974); N. Kimizuka and T. Katsura, J. Solid State Chem. **13**, 176 (1975).

[4] N. Ikeda, K. Kohn, H. Kito, J. Akimitsu, and K. Siratori, J. Phys. Soc. Jpn. **63**, 4556 (1994).

[5] N. Ikeda, K. Kohn, H. Kito, J. Akimitsu, and K. Siratori, J. Phys. Soc. Jpn. **64**, 1371 (1995).

[6] N. Ikeda, K. Kohn, N. Myouga, E. Takahashi, H. Kitoh, and S. Takekawa, J. Phys. Soc. Jpn. **69**, 1526 (2000).

[7] K. Yoshiia, N. Ikeda, and A. Nakamura, Physica B **378-380**, 585 (2006).

[8] M. A. Subramanian, T. He, J. Z. Chen, N. S. Rogado, T. G. Calvarese, and A. W. Sleight, Adv. Mater. Weinheim, Ger. **18**, 1737 (2006).

[9] M. Isobe, N. Kimizuka, J. Iida, and S. Takekawa, Acta Crystallogr. C **46**, 1917 (1990).

[10] J. Blasco, S. Lafuerza, J García, and G. Subías, Phys. Rev. B **90**, 094119 (2014).

[11] Y. Nagakawa, M. Inazumi, N. Kimizuka, and K. Siratori, J. Phys. Soc. Jpn. **47**, 1369 (1979).

[12] M. Tanaka, J. Akimitsu, Y. Inada, N. Kimizuka, I. Shindo, and K. Siratori, Solid State Commun. **44**, 687 (1982).

[13] J. Iida, Y. Nakagawa, S. Takekawa, and N. Kimizuka, J. Phys. Soc. Jpn. **56**, 3746 (1987).

[14] J. Iida, M. Tanaka, Y. Nakagawa, S. Funahashi, N. Kimizuka, and S. Takekawa, J. Phys. Soc. Jpn. **62**, 1723 (1993).

[15] M. Kishi, S. Miura, Y. Nakagawa, N. Kimizuka, I. Shindo, and K. Siratori, J. Phys. Soc. Jpn. **51**, 2801 (1982).

[16] K. Yoshii, N. Ikeda, and S. Mori, J. Magn. Magn. Mat. **310**, 1154 (2007).

[17] N. Ikeda, H. Ohsumi, K. Ohwada, K. Ishii, T. Inami, K. Kakurai, Y. Murakami, K. Yoshii, S. Mori, Y. Horibe, and H. Kito, Nature (London) **436**, 1136 (2005).

[18] A. M. Mulders, S. M. Lawrence, U. Staub, M. Garcia-Fernandez, V. Scagnoli, C. Mazzoli, E. Pomjakushina, K. Conder, and Y. Wang, Phys. Rev. Lett. **103**, 077602 (2009).

[19] H. J. Xiang and M.-H. Whangbo, Phys. Rev. Lett. **98**, 246403 (2007).

[20] A. Nagano, M. Naka, J. Nasu, and S. Ishihara, Phys. Rev. Lett. **99**, 217202 (2007).

[21] Y. Zhang, H. X. Yang, Y. Q. Guo, C. Ma, H. F. Tian, J. L. Luo, and J. Q. Li, Phys. Rev. B **76**, 184105 (2007).

[22] W. Wu, V. Kiryukhin, H.-J. Noh, K.-T. Ko, J.-H. Park, W. Ratcliff II, P. A. Sharma, N. Harrison, Y. J. Choi, Y. Horibe, S. Lee, S. Park, H. T. Yi, C. L. Zhang, and S.-W. Cheong, Phys. Rev. Lett. **101**, 137203 (2008).

[23] A. D. Christianson, M. D. Lumsden, M. Angst, Z. Yamani, W. Tian, R. Jin, E. A. Payzant, S. E. Nagler, B. C. Sales, and D. Mandrus, Phys. Rev. Lett. **100**, 107601 (2008).

[24] M. Angst, R. P. Hermann, A. D. Christianson, M. D. Lumsden, C. Lee, M.-H. Whangbo, J.-W. Kim, P. J. Ryan, S. E. Nagler, W. Tian, R. Jin, B. C. Sales, and D. Mandrus, Phys. Rev. Lett. **101**, 227601 (2008).

[25] X. S. Xu, M. Angst, T. V. Brinzari, R. P. Hermann, J. L. Musfeldt, A. D. Christianson, D. Mandrus, B. C. Sales, S. McGill, J.-W. Kim, and Z. Islam, Phys. Rev. Lett. **101**, 227602 (2008).

[26] F. Wang, J. Kim, and Y.-J. Kim, Phys. Rev. B **80**, 024419 (2009).

[27] K.-T. Ko, H.-J. Noh, J.-Y. Kim, B.-G. Park, J.-H. Park, A. Tanaka, S. B. Kim, C. L. Zhang, and S-W. Cheong, Phys. Rev. Lett. **103**, 207202 (2009).

[28] C.-H. Li, F. Wang, Y. Liu, X.-Q. Zhang, Z.-H. Cheng, and Y. Sun, Phys. Rev. B **79**, 172412 (2009).

[29] J. S. Wen, G. Y. Xu, G. Gu, and S. M. Shapiro, Phys. Rev. B **80**, 020403(R) (2009).

[30] K. Kuepper, M. Raekers, C. Taubitz, M. Prinz, C. Derks, M. Neumann, A. V. Postnikov, F. M. F. de Groot, C. Piamonteze, D. Prabhakaran, and S. J. Blundell, Phys. Rev. B **80**, 220409(R) (2009).

[31] A. B. Harris and T. Yildirim, Phys. Rev. B **81**, 134417 (2010).

[32] J. Rouquette, J. Haines, A. Al-Zein, P. Papet, F. Damay, J. Bourgeois, T. Hammouda, F. Dore, A. Maignan, M. Hervieu, and C. Martin, Phys. Rev. Lett. **105**, 237203 (2010).

[33] X. S. Xu, J. de Groot, Q.-C. Sun, B. C. Sales, D. Mandrus, M. Angst, A. P. Litvinchuk, and J. L. Musfeldt. Phys. Rev. B **82**, 014304 (2010).

[34] B. Fisher, J. Genossar, L. Patlagan, and G. M. Reisner, J. Appl. Phys. **109**, 084111 (2011).

[35] A. M. Mulders, M. Bartkowiak, J. R. Hester, E. Pomjakushina, and K. Conder, Phys. Rev. B **84**, 140403(R) (2011).

[36] M. Bartkowiak, A. M. Mulders, V. Scagnoli, U. Staub, E. Pomjakushina, and K. Conder, Phys. Rev. B **86**, 035121 (2012).

[37] J. de Groot, K. Marty, M. D. Lumsden, A. D. Christianson, S. E. Nagler, S. Adiga, W. J. H. Borghols, K. Schmalzl, Z. Yamani, S. R. Bland, R. de Souza, U. Staub, W. Schweika, Y. Su, and M. Angst, Phys. Rev. Lett. **108**, 037206 (2012).

[38] J. de Groot, T. Mueller, R. A. Rosenberg, D. J. Keavney, Z. Islam, J.-W. Kim, and M. Angst, Phys. Rev. Lett. **108**, 187601 (2012).

[39] D. Niermann, F. Waschkowski, J. de Groot, M. Angst, and J. Hemberger, Phys. Rev. Lett. **109**, 016405 (2012).

[40] A. Ruff, S. Krohns, F. Schrettle, V. Tsurkan, P. Lunkenheimer, and A. Loidl, Eur. Phys. J. B **85**, 290 (2012).

[41] S. Lafuerza, J. García, G. Subías, J. Blasco, K. Conder, and E. Pomjakushina, Phys. Rev. B **88**, 085130 (2013).

[42] S. Lafuerza, J. García, G. Subías, J. Blasco, and V. Cuartero, Phys. Rev. B **89**, 045129 (2014).

[43] S. Lafuerza, G. Subías, J. Blasco, J. García, G. Nisbet, K. Conder, and E. Pomjakushina, Europhys. Lett. **107**, 47002 (2014).

[44] S. Lafuerza, G. Subías, J. Blasco, J. García, G. Nisbet, K. Conder, and E. Pomjakushina, Phys. Rev. B **90**, 085130 (2014).

[45] G. Subías, J. García, J. Blasco, J. Herrero-Martín, M. C. Sánchez, J. Orna, and L. Morellón, J. Synchr. Rad. **19**, 159 (2012).

[46] G. Subías, J. García, J. Blasco, J. Herrero-Martín, and M. C. Sánchez, J. Phys. Conf. Series **190**, 012085 (2009).

[47] http://www.cells.es/en/beamlines/bl29-boreas.

[48] S. Pascarelli, O. Mathon, M. Muñoz, T. Mairs, and J. Susini, J. Synchr. Rad. **13**, 351 (2006).

[49] Y. Joly, Phys. Rev. B **63**, 125120 (2001).

[50] F. M. F. de Groot and A. Kotan, *Core Level Spectroscopy of Solids* (Taylor & Francis CRC, Boca Raton, FL, 2008).

[51] E. Stavitski and F. M. F. de Groot, Micron **41**, 687 (2010).

[52] Z. Y. Wu, S. Gota, F. Jollet, M. Pollak, M. Gauitier-Soller, and C. R. Natoli, Phys. Rev. B **55**, 2570 (1997).

[53] S. Lafuerza, G. Subías, J. García, S. Di Matteo, J. Blasco, V. Cuartero, and C. R. Natoli, J. Phys.: Condens. Matter **23**, 325601 (2011).

[54] M. Abbate, F. M. F. De Groot, J. C. Fuggle, A. Fujimori, O. Strebel, F. Lopez, M. Domke, G. Kaindl, G. A. Sawatzky, M. Takano, Y. Takeda, H. Eisaki, and S. Uchida, Phys Rev B **46**, 4511 (1992).

[55] J. P. Crocombette, M. Pollak, F. Jollet, N. Thromat, and M. Gautier-Soyer, Phys. Rev. B **52**, 3143 (1995).

[56] T. J. Regan, H. Ohldag, C. Stamm, F. Nolting, J. Lüning, J. Stöhr, and R. L. White, Phys. Rev. B **64**, 214422 (2001).

[57] F. M. F. De Groot, P. Glatzel, U. Bergmann, P. A. van Aken, R. A. Barrea, S. Klemme, M. Hävecker, A. Knop-Gericke, W. M. Heijboer, and B. M. Weckhuysen, J. Phys. Chem. B **109**, 20751 (2005).

[58] F. Sette, C. T. Chen, Y. Ma, S. Modesti, and N. V. Smith, in *X-Ray Absorption Fine Structure*, edited by S. S. Hasnain (Ellis Horwood, New York, 1991).

[59] C. T. Chen, Y. U. Idzerda, H.-J. Lin, N. V. Smith, G. Meigs, E. Chaban, G. H. Ho, E. Pellegrin, and F. Sette, Phys. Rev. Lett. **75**, 152 (1995).

[60] D. J. Huang, C. F. Chang, H.-T. Jeng, G. Y. Guo, H.-J. Lin, W. B. Wu, H. C. Ku, A. Fujimori, Y. Takahashi, and C. T. Chen, Phys. Rev. Lett. **93**, 077204 (2004); We note that in this paper the sum rules analysis agrees with the macroscopic magnetization after taken erroneously the number of holes per formula unit instead of the number of holes per atom.

[61] E. J. Goering, M. Lafkioti, S. Gold, and G. Schuetz, J. Magn. Magn. Mater. **310**, e249 (2007).

[62] M. Tanaka, H. Iwasaki, K. Siratori, and I. Shindo, J. Phys. Soc. Jpn. **58**, 1433 (1989).

[63] L. Tröger, D. Arvanitis, K. Baberschke, H. Michaelis, U. Grimm, and E. Zschech, Phys. Rev. B **46**, 3283 (1992).